

## Improving Reliability of Isolated Microgrid-based Solar Energy Using Fuzzy Controlled-Flywheel Energy Storage

Abdelkader Omar, Mohamed M. Aly, Salah Kamel, Mouaz Zobair, and Sayed M. Said

Department of Electrical Engineering, Aswan University, Aswan 81542, Egypt.

### Abstract

Islanded microgrids (MGs) deliver essential electrical power to remote areas utilizing renewable energy sources (RESs). The most common RES is solar power generation (SPG). Still, these systems have several serious issues with the natural conditions of temperature and solar radiation, which reduces the reliability of the MG and may negatively affect the voltage level and frequency regulation. Energy storage techniques are important in overcoming the above issues with the island MGs. This study presents an effective control method to improve the performance of the islanded MG during normal operation and critical circumstances by employing a flywheel energy storage system (FESS) based on a fuzzy logic controller (FLC). Three scenarios are examined at different solar radiation conditions and load demand with the MATLAB/Simulink platform. Regarding Scenario 3, as a worst case, the percentages of the minimum undershoot and maximum overshoot frequency values are 4.18% and 1.1% in the case without FESS, respectively, where these are 0.98% and 0.32% with FESS, respectively. On the other hand, the percentages of the minimum undershoot, and maximum overshoot values of the common connection point (CCP) voltage can be reduced from 2.3% and 6.3% without using FESS to 0.79% and 5% when using FESS, respectively. The simulation results demonstrate that the suggested method is superior at reducing frequency and voltage fluctuations, and the dependence on the diesel generator is reduced.

**Keywords:** hybrid generation systems; isolated Microgrid; photovoltaic; flywheel storage system; fuzzy logic controller.

### Introduction

The world economy is developing quickly, which has led to a rapid rise in energy demand. The nature of fossil fuel energy resources such as coal, oil, and natural gas is that they are nonrenewable and have negative effects on the environment [1], [2]. To overcome these problems, the penetration of renewable energy sources (RESs) has become the most priority issue in different countries worldwide. Therefore, many agreements have been signed to increase the contribution of RESs and secure a sustainable energy future [3], [4]. RESs are crucial in constructing a sustainable future; it is anticipated to increase from 11% now to 28% of total primary energy consumed globally by 2050 [5].

The microgrid (MG) is defined as a combination of different renewable and nonrenewable resources operating together efficiently to handle local loads. MGs can operate in both grid-connected and islanded mode [6]. People in remote areas face many difficulties while they seek to save their electricity demand for different purposes. Transmission of electricity to remote areas has many problems in addition to its high cost [7]. Hybrid RESs are regarded as the preferred option to provide electricity demands for remote areas [8]. Hybrid RESs contain different distributed generators to satisfy consumers' power demands. For example, the integration between diesel generators, as a conventional source of energy, and RESs such as photovoltaic (PV) and wind energy using effective types of energy storage systems (ESSs) constitute hybrid RES [6].

\*Corresponding author E-mail: [abdelkader.omar@eng.aswu.edu.eg](mailto:abdelkader.omar@eng.aswu.edu.eg)

Received November 03, 2024, received in revised form, December 15, 2024, accepted December 15, 2024.

PV energy converts energy from the sun to electrical power, and in the present time, it has undergone great development due to advanced material technologies [9]. PV system costs have decreased quickly because of the substantial economies of scale that have also been attained [10]. The total installed capacity worldwide is expected to increase from 1.0 TW in 2022 up to 5.042 TW in 2030 [11], [12].

The intermittent nature of RESs, such as PV and wind, makes the application of ESSs in Hybrid RESs becoming more important [13]. Weather conditions are generally affecting the power output from PV and wind. In calm conditions, the output power capacity of wind turbines decreases, and the output power of PV decreases during cloudy days [14]. To overcome these problems, ESSs are employed, charging when the energy demand is less and discharging when the energy demand is high. ESSs are means of transferring electrical energy from the electrical power network into a form that may be stored and then used again when necessary [15].

ESSs have many applications in power systems, such as power quality and grid stabilization [6]. There are many types and technologies for energy storage, such as flywheel energy storage systems (FESSs) [16], [17], compressed air [18], thermal energy storage [19], supercapacitors [20], and pumped hydro [21]. These technologies can be compared according to specific power, specific energy, charging and discharging time, response time, service life, cost, and efficiency. Authors in [6], [14], [22] have provided a detailed comparison between the different types of ESSs.

FESS is a type of ESS that has a fast response and can deliver a large amount of power in a short time reaching a fraction of a second. It also has high efficiency and long lifetime [23]. Furthermore, its standby losses are low; from a few minutes to a few hours compared to other types of ESSs [24]. FESS has been applied for different applications such as aircraft and military projects, hybrid vehicles, RES integration, power smoothing, power quality improvements, uninterruptible power supply (UPS) systems, flexible AC transmission systems (FACTS), and stability improvement [17], [23].

Many studies have been proposed by many researchers to study PV and FESS integration. In [25], an experimental test has been conducted to examine how the FESS can be applied in PVs to improve the voltage control issue that arises at low loads. The test is applied at different FESS speeds. In [26], the FESS and PV were coordinated to improve the system's reliability. In [27], FESS has been used in combination with PV power generation to mitigate the fluctuation of solar energy. Furthermore, in [28], a system consisting of PV panels and micro-FESS has been studied to show that FESS can help in compensating variation of PV power generation based on a suitable control strategy.

This study focuses on the integration of diesel generators, PV, and FESS. Three scenarios are studied with and without FESS by changing the load and solar radiation profiles to illustrate the effect of FESS in improving the MG performance. A fuzzy logic controller (FLC) strategy is utilized for controlling the charging/discharging of FESS. The main contributions of this study can be summarized as follows:

- Analyzing the integration of solar power generation (SPG) with FESS in an isolated MG system to improve reliability.
- Using FLC to enhance the charging/discharging process of the FESS.

- Mitigating the voltage and frequency fluctuations caused by weather conditions and sudden load demand variation by installing a FESS into the MG.
- Reducing the output power of the diesel generator which can decrease the total power losses.

## Mathematical Model of MG System

### MG System and Modeling of Solar Power Generation (SPG)

Figure 1 shows the complete structure of the studied system, which consists of PV, FESS, diesel generator, and local load. Solar PV is made up of PV modules, a DC-DC boost converter, a voltage source inverter (VSI), and a step-up transformer. The first stage of the construction of a PV system is to select a PV module so that installation costs and overall system efficiency are taken into consideration. In this study, the Jinko Solar MONO-FACIAL MODULE (JKM550M-72HL4) with a maximum output power of 550 W at standard test conditions (STC) was selected as the PV module to be used to build the proposed PV system. Table 1. provides the electrical specifications of the PV module. The proposed PV system is composed of one PV array. To implement a PV array, PV modules are connected in series ( $N_S$ ), and parallel ( $N_P$ ) to get the required PV output power.

To determine the value of  $N_S$ , the DC link reference voltage of the PV system is calculated. The minimum value of DC link voltage can be calculated using (1) [29], where the value of  $V_{Phase, RMS}$  is 230 V.

$$V_{DC\ link} \geq 2\sqrt{2} V_{Phase, RMS} \quad (1)$$

By substituting in (1), the  $V_{DC\ link} \cong 653.2$  V. Practically, the DC link voltage is taken as 700 V. So,  $N_S$  can be calculated using (2);  $V_{MP}$  is the value of maximum power voltage from Table 1, so the value of  $N_S$  is calculated as follows:

$$N_S = 0.5 \times \left( \frac{V_{DC\ Link}}{V_{MP}} \right) \cong 9 \quad (2)$$

The PV array output power at STC can be calculated using (3). Because the required output power is 1.0 MW, the value of  $N_P = 202$ .

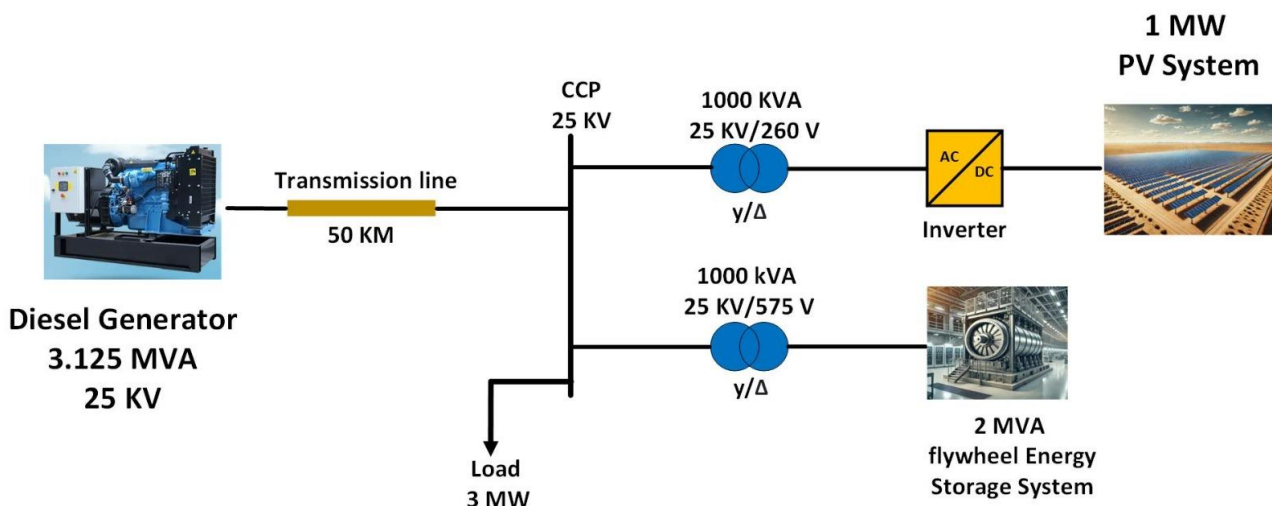
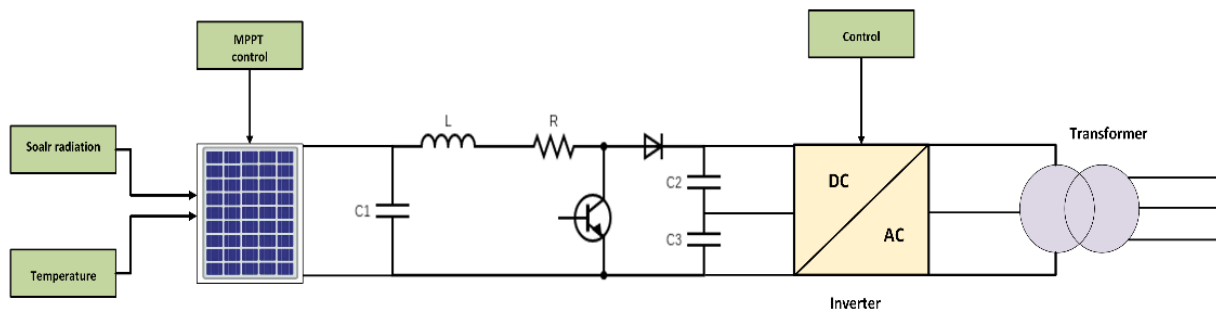


Figure 1. Single-line diagram for the studied system.



**Figure 2. The schematic diagram of SPG.**

$$P_{PVarray,STC} = (N_S * N_P) \times P_{max,STC} \quad (3)$$

The output PV power is directly affected by weather conditions like solar radiation, temperature, dust, wind, and humidity [30]. Temperature and solar radiation are more prominent factors that affect PV output power; other conditions are neglected in this study. The output power of a PV array can be calculated using (4) [31], [32].

$$PV_{output} = PV_{array,STC} \times f_{PV} \times \left( \frac{G_T}{G_{STC}} \right) \times [1 + \alpha(T_c - T_{c,STC})] \quad (4)$$

where  $T_c$ ,  $T_{c,STC}$ , and  $G_{STC}$  represent cell temperature and solar radiation at STC, respectively, and their values are 25 °C and 1000 W/m<sup>2</sup>.  $f_{PV}$  is the derating factor for the PV system, and  $\alpha$  is the coefficient.  $G_T$  and  $T_c$  are solar radiation and temperature during system operation.  $PV_{output}$  and  $PV_{array,STC}$  represent PV output power and PV array output power.

In this study, the temperature is taken as 25 °C, and solar radiation is studied in different conditions.

A DC-DC boost converter is used to boost the DC output voltage of the PV array up to 1000 V and produce a constant output voltage regardless of the fluctuations in the input voltage. Maximum power point tracking (MPPT) is employed to enhance system efficiency and gain the maximum power from PV modules [33]. Many techniques were considered for MPPT, like PI control, constant voltage, incremental conductance, perturb and observe (P&O), and fuzzy logic methods [34]. In this study, the DC-DC converter is based on PI control. The parameters of the DC-DC converter and controller are summarized in Table 2. The output from the DC-DC converter is converted to three-phase AC voltage using a Voltage source inverter (VSI). The model of the PV system is connected to CCP through a 0.260Δ/25Y kV step-up transformer. The schematic of the complete SPG system is illustrated in Figure 2. The parameters of the DC-DC converter and its control are summarized in Table 2.

### **Flywheel energy storage system (FESS)**

FESS converts electric energy into mechanical energy as kinetic energy. The energy input to the flywheel can be provided by an electrical source, such as the grid or any other electrical energy source. The main components of the flywheel are the rotor, electrical machine (motor-generator), bearings, power electronics, and housing, as shown in Figure 3. Further details on the description of each component are addressed in [17], [35], [36].

TABLE 1. THE ELECTRICAL Specifications OF THE PV MODULE

Module type	JKM550M-72HL4-V
PV module max power ( $P_{max}$ )	550 w
Maximum Power Voltage ( $V_{mp}$ )	40.90 V
Maximum Power Current ( $I_{mp}$ )	13.45 A
Open-circuit Voltage ( $V_{oc}$ )	49.62 V
Short-circuit Current ( $I_{sc}$ )	14.03 A
Operating Temperature ( $^{\circ}C$ )	-40 $^{\circ}C$ ~+85 $^{\circ}C$
Maximum system voltage	1000/1500VDC (IEC)
Power Tolerance	0~+3%
Temperature coefficients of $P_{max}$	-0.35%/ $^{\circ}C$
Temperature coefficients of $V_{oc}$	0.28%/ $^{\circ}C$
Temperature coefficients of $I_{sc}$	0.048%/ $^{\circ}C$
Nominal operating cell temperature (NOCT)	45 $\pm$ 2 $^{\circ}C$

TABLE 2. PARAMETERS OF DC-DC CONVERTER AND CONTROLLER

C1	325 $\mu$ F
C2	70 mF
C3	70 mf
Total transformer leakage impedance [ $R_{xfo}$ $L_{xfo}$ ]	[0.002 0.06] (p.u./Pnom)
Choke impedance [ $R_{chock}$ , $L_{chock}$ ]	[2e-3 $\Omega$ , 250e-6 H]
Nominal DC bus voltage	1000 V
VSI switching frequency	1980 Hz
MPPT switching frequency	5 kHz
VSI rated	1000 KVA
VDC controller PI-1 [ $K_p$ $K_i$ ]	[7 800]
Current controllers PI-2, PI-3 [ $K_p$ $K_i$ ]	[0.3 20]

Flywheel has three modes of operation: charging, discharging, and holding mode. In charging mode, the machine operates as a motor and converts the electrical energy into kinetic energy. In discharging mode, the machine operates as a generator and converts the stored energy into electrical energy. Holding mode is achieved when the flywheel reaches its target speed so, in this case, there is no energy transfer to/from the flywheel [35].

The maximum stored kinetic energy in a flywheel  $E$  (J) that has a moment of inertia  $J$  (Kg.m<sup>2</sup>) and rotates with angular velocity  $\omega$  (rad/s) can be given by (5) [37], [38].

$$E = \frac{1}{2} J \omega^2 \quad (5)$$

The only portion of this energy is usable, and is given by (6):

$$E = \frac{1}{2} J (\omega_{max}^2 - \omega_{min}^2) = \frac{1}{2} J \omega_{max}^2 \left( 1 - \frac{\omega_{min}^2}{\omega_{max}^2} \right) \quad (6)$$

To avoid excessive voltage variations due to design consideration for machine size, the flywheel speed range is between maximum speed ( $\omega_{max}$ ) and minimum speed ( $\omega_{min}$ ), namely 0.3 to 0.5 of flywheel rated speed, respectively [38].

In FESS, the main component is the electrical machine. Many types can be employed, like the permanent magnet synchronous machine (PMSM), the double-fed inductor machine (DFIM), and the squirrel cage inductor machine (SCIM). In this study, the FESS is based on DFIM. Further details on the modeling of DFIM are expressed in [39], [40], [41]. The main characteristics of rotor flywheel materials are discussed in detail in [17]. Improving flywheel density mainly depends on developing rotor material used in flywheels. The integration of FESS with PV systems is studied in [38], [42].

In this study, FESS has a power rating of 2 MVA and an energy rating of 50 MJ. The inertia constant and rated speed are 705 (kg.m<sup>2</sup>) and 377 (rad/sec), respectively.

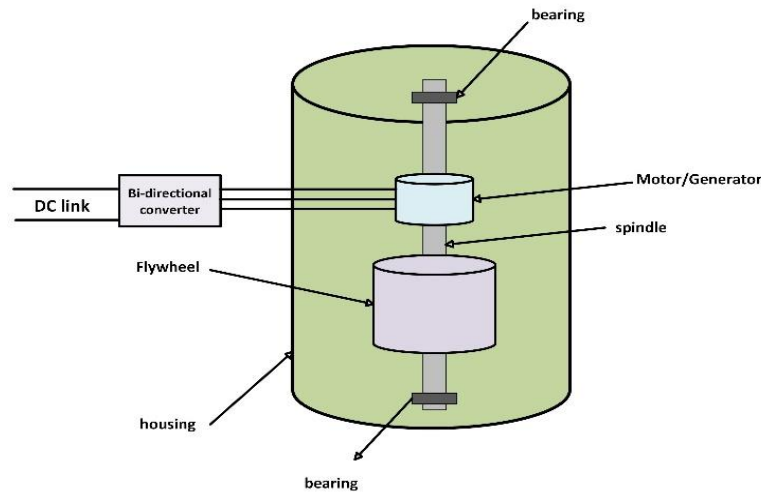


**Figure 3. The structure of FESS.**

### ***Proposed Method Based on Fuzzy Control***

The FLC strategy, utilized in the proposed method to control the FESS in the hybrid MG system, consists of five main elements:

- Fuzzification module.
- Knowledge base.
- Rule base.
- Inference engine.
- Defuzzification module.

Figure 4 illustrates the block diagram of an FLC [43], [44], [45]. The internal design of these elements determines the effectiveness of FLC. The main function of the fuzzification module is to convert the crisp values of the control inputs into fuzzy values. The knowledge base includes a plant database; it also gives definitions required for the fuzzification process as membership functions (MFs) and fuzzy set representations of the input and output variables. The rule base is the control strategy for the system, and it is derived from heuristics or expert knowledge and presented as a series of IF-THEN rules. An inference engine is used to combine the measured parameters with the controlled ones depending on fuzzy rules. The defuzzification module converts fuzzy values into crisp values [46], [47], [48].

The main process in designing FLC is to define controller inputs and output variables. In this study, FLC consists of two inputs and one output. The difference between PV output power and load power

( $dP$ ) and the FESS current speed's variation from its rated speed ( $d\omega$ ) are the input variables, where  $dP$  and  $d\omega$  can be defined as follows:

$$dP = P_{PV} - P_{Load} \tag{7}$$

$$d\omega = 1 - \frac{\omega_f}{\omega_r} \tag{8}$$

where:  $P_{PV}$ ,  $P_{Load}$ ,  $\omega_f$  and  $\omega_r$  are the PV output power, load power, flywheel current speed, and flywheel-rated speed, respectively.

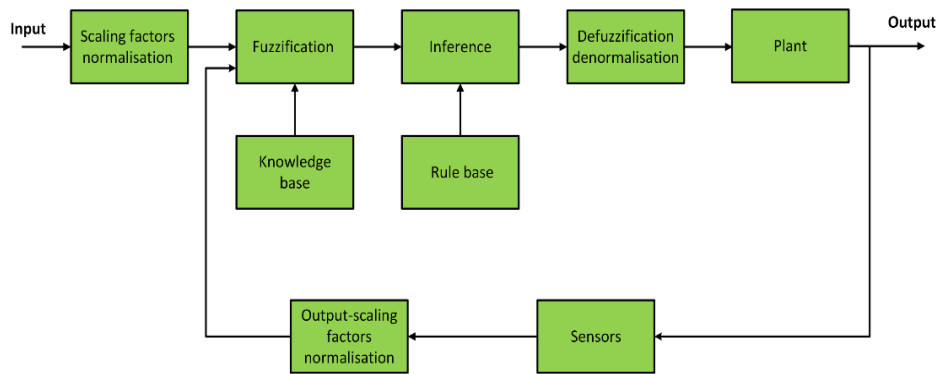


Figure 4. The block diagram of FLC

The control output signal is the reference power ( $P_{ref}$ ), and it is utilized as the flywheel voltage source converter's input. The range for ( $P_{ref}$ ) is [-10:10] MW. The maximum shareable power for FESS is 2 MW. Figure 5 shows the MFs of inputs and output variables.

The selection of MFs, such as their distribution, number, and shape, is important in designing FLC because they indicate the degree of truth. In this study, each controller variable is represented by seven sets of Gaussian MFs where there are 49 inference rules, as summarized in Table 3.

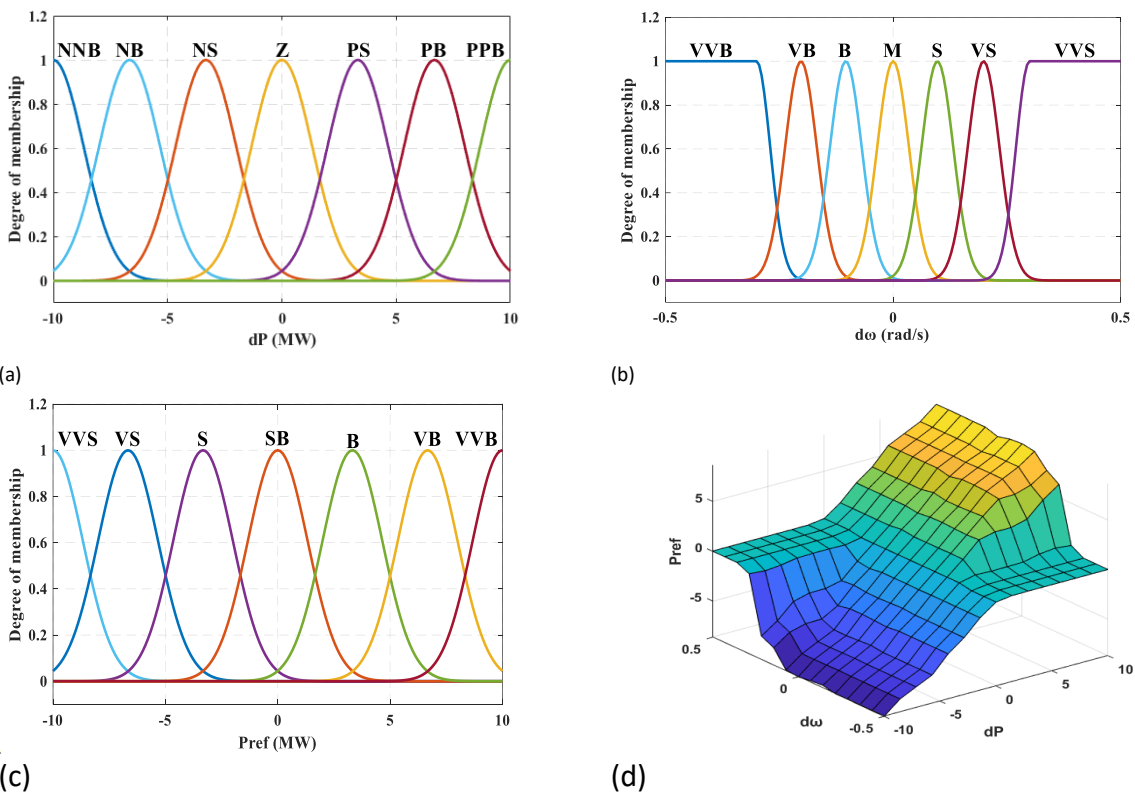


Figure 5. MFs of FLC. (a)  $dP$ , (b)  $d\omega$ , (c) the output variable ( $P_{ref}$ ), (d) 3-D control surface.

**TABLE 3. Rules base table for the proposed FLC**

$\begin{matrix} dP \\ d\omega \end{matrix}$	VVB	VB	B	M	S	VS	VSS
NNB	VSS	VSS	VSS	VSS	VSS	VS	SB
NS	S	S	S	S	S	S	SB
Z	SB						
PS	SB	B	B	B	B	B	B
PPB	SB	VB	VVB	VVB	VVB	VVB	VB
NB	VS	VS	VS	VS	VS	S	VVB
PB	SB	B	VB	VB	VB	VB	VB

## Results and Discussion

As presented in Fig. 1, the isolated MG consists of a solar PV system with a capacity of 1.0 MW, a 2 MVA FESS, and a 3.125 MVA diesel generator (DG). Power converters and transformers are utilized to connect solar PV and FESS to the common connection point (CCP). A 50-km-long transmission line is used to connect DG to CCP to supply a 3 MW local load.

In this study, the effects of integrating FESS into an MG with a diesel generator and PV are studied. The main function is to reduce diesel generator power contribution in the system to eliminate environmental effects. It is suggested that FESS increases the overall system reliability by decreasing generator-sharing power and overcoming any gap between the load demand and the total generation.

The size of all MG components is taken the consideration to supply the load regardless of any change in surrounding conditions. FESS compensates for the difference between generation and load due to the intermittent nature of PV power. FLC is applied to the FESS as a proposed control to compensate for the gap between generation and load demand.

The MG system in Figure 1 is tested for three different scenarios to ensure the effectiveness of the control strategy. The studied system is built in MATLAB/Simulink, and the results are carried out in two cases (with and without FESS).

### Scenario 1

In this scenario, the applied solar radiation, output PV power, and load profile are shown in Figures 6a - 6c, respectively. The system frequency and voltage at CCP are presented in Figures 7a and 7b. The primary frequency value while using FESSs is 59.7 Hz, which is quite near to the system frequency of 60 Hz. On the other hand, when FESS is not being used, the lowest frequency values are approximately 58.8 Hz and 59.11 Hz at different times. During operation, the load is immediately impacted by frequency fluctuations. The voltage at CCP is shown in Figure 7b. When FESS is used, the variation that occurs at time = 2 s and t = 5 s is somewhat less than when FESS is not used.

Figure 8 discusses the diesel generator's active power, reactive power, and rotor speed. With the same amount of power shared via FESS, it is found that the diesel generator's active power share drops. Using FESS results in reactive power that is almost zero. Using FESS results in a rotor speed of about 1.0 pu, compared with oscillation between maximum and minimum values of 1.014 pu and 0.985 pu, respectively without using FESS.

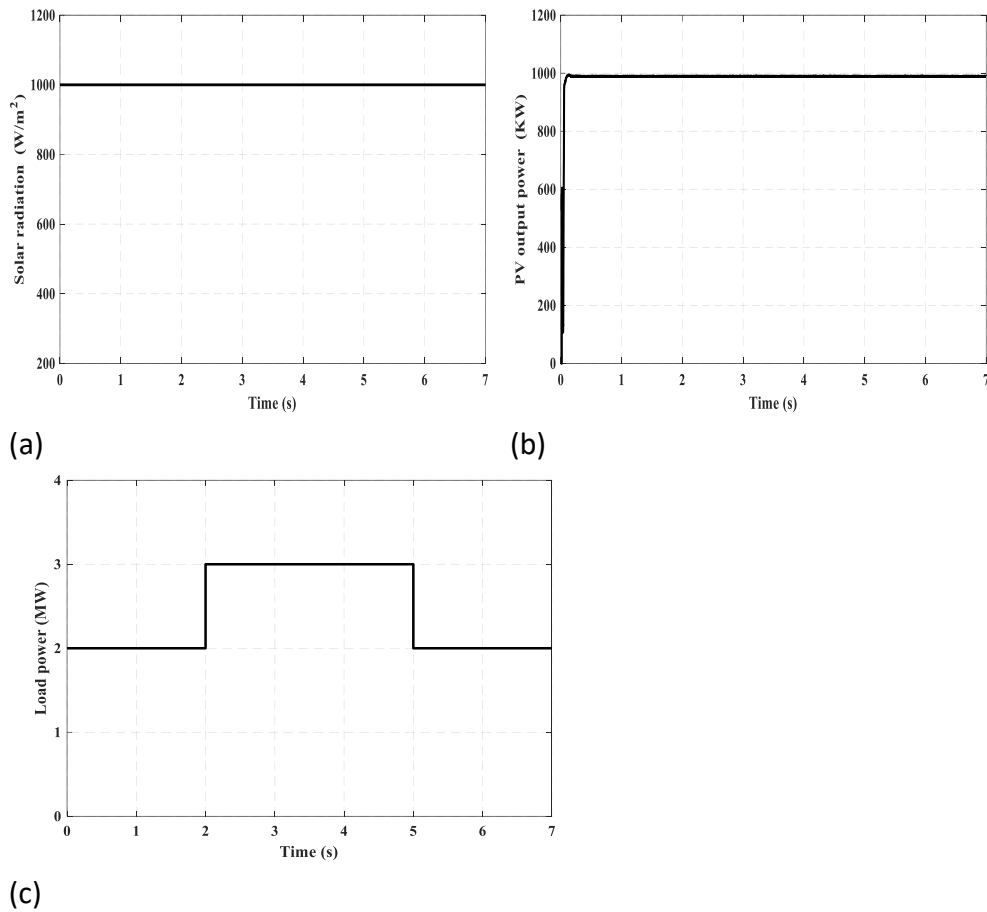


Figure6. (a) Solar radiation for Scenario 1, (b) PV power for Scenario 1, (c) Load profile for Scenario 1.

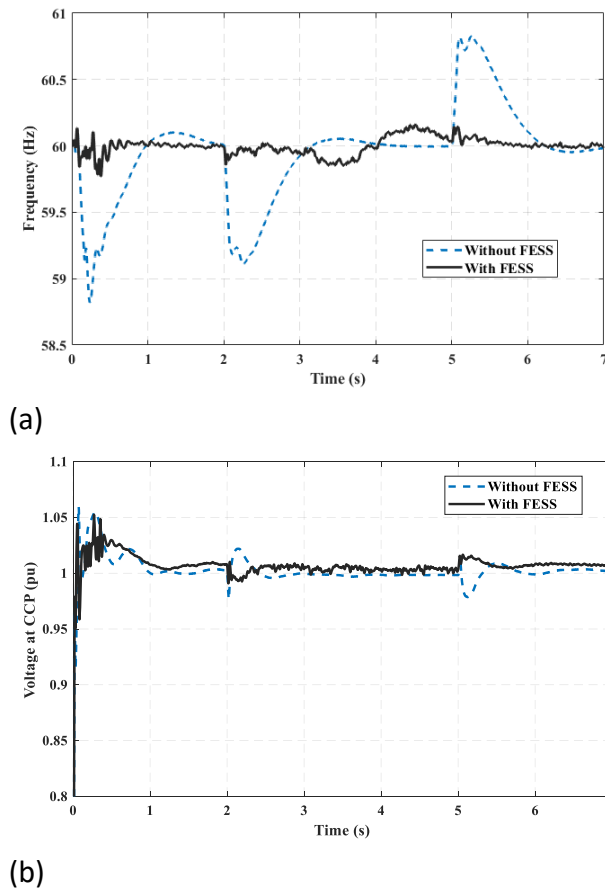


Figure7. (a) System frequency of Scenario1, (b) Voltage at CCP of Scenario1.

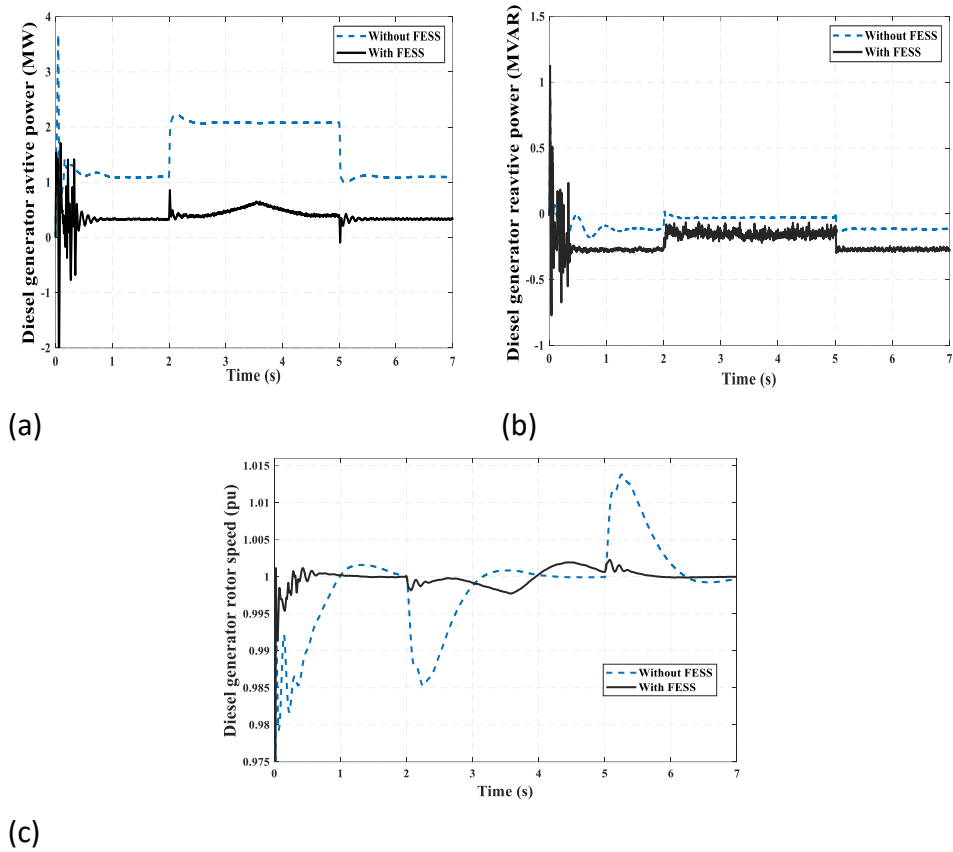


Figure 8. (a) Diesel generator active power of Scenario1, (b) Diesel generator reactive power of Scenario1, (c) Diesel generator rotor speed of Scenario1.

Figure 9 shows the FESS output's active and reactive powers, while Figure 10 illustrates the FESS's energy, speed, and DC voltage. FESS makes a substantial contribution to feeding the expected load. When charging or discharging, FESS reacts quickly to accommodate any unexpected change in load demand.

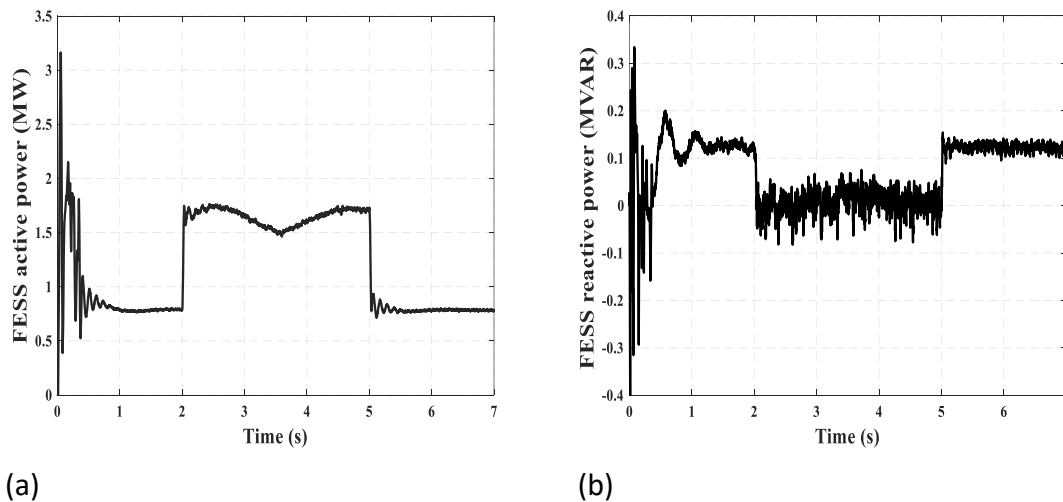
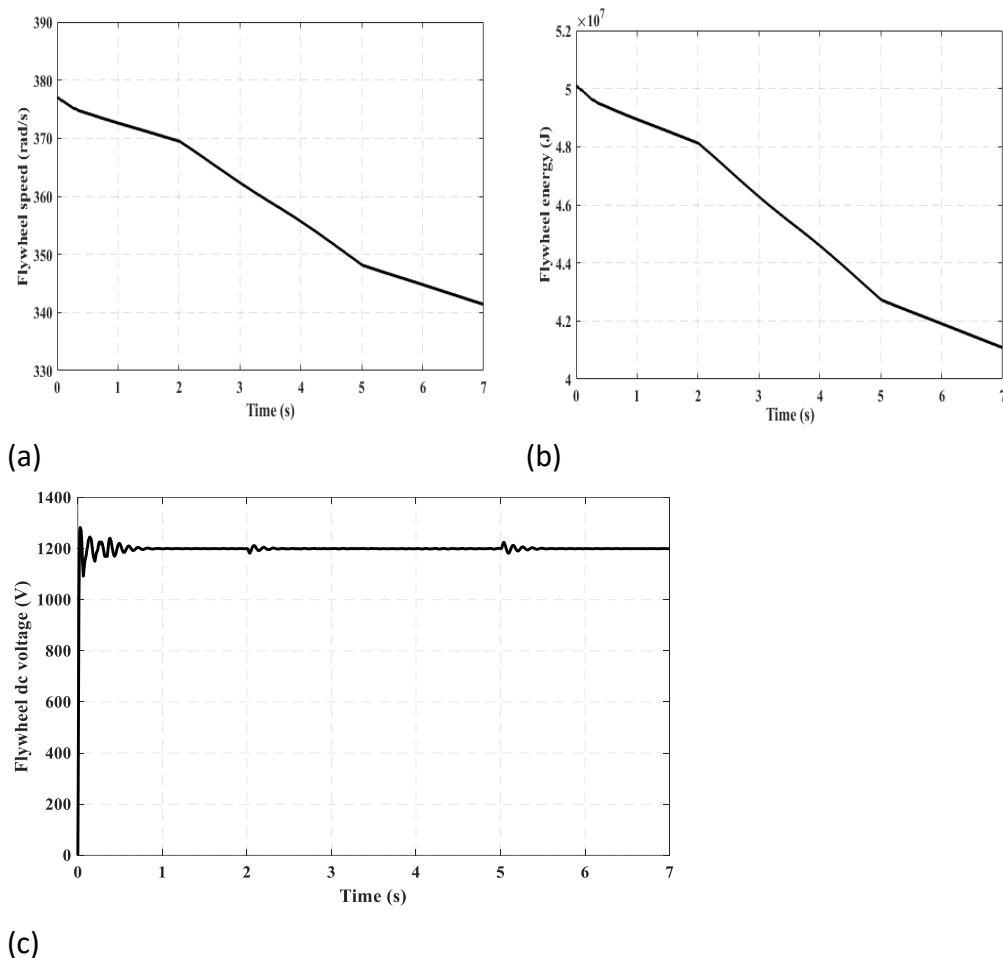


Figure 9. (a) FESS active power output of Scenario 1, (b) FESS reactive power output of Scenario 1.



**Figure 10. (a) Flywheel speed of Scenario1, (b) FESS energy of Scenario1, (c) Flywheel dc voltage of Scenario1.**

### Scenario 2

In this scenario, the profile of solar radiation, PV output power, and the load profile are shown in Figures 11a - 11c, respectively. Figure 12 displays the MG system frequency; frequency values are within acceptable bounds when FESS is used. FESS eliminates the negative impact of the minimum frequency of 57.94 Hz, which occurs when FESS is not applied. The voltage at CCP is shown in Figure 13. When FESS is not employed, the voltage at CCP is kept constant at 0.99 pu; however, when FESS is used, the value is roughly 1.0 pu, which is regarded as a significant improvement in system voltage.

The active power, reactive power, and rotor speed of the diesel generator are covered in Figure 14. The diesel generator's active power share is observed to decrease with the same amount of power transferred via FESS. Reactive power is nearly negligible when using FESS. A rotor speed of roughly 1.0 pu is achieved by employing FESS compared with values between 1.005 pu and 0.965 pu without using FESS. The FESS output's active power, reactive power, FESS energy, speed, and DC voltage are displayed in Figures 15a–15c, respectively. FESS plays a significant role in feeding the anticipated load. Any sudden change in load demand is accommodated by FESS's rapid response while charging or discharging.

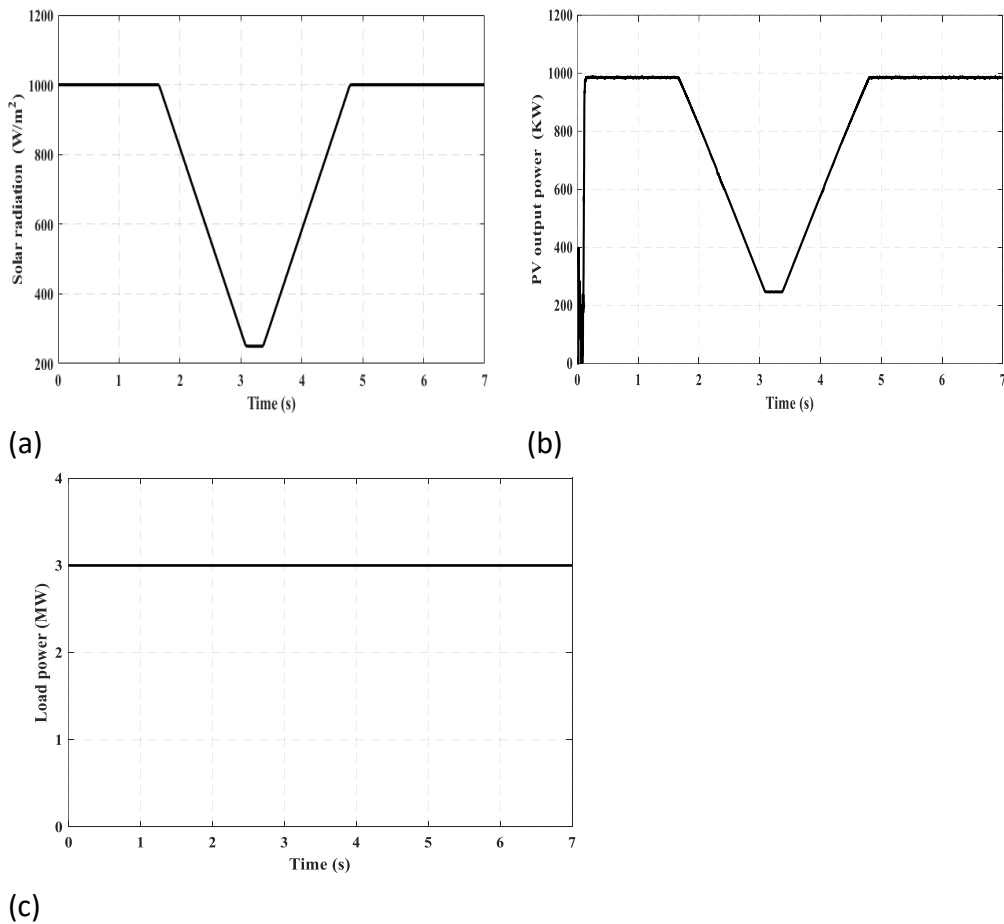


Figure 11. (a) Solar radiation for Scenario 2 and 3, (b) PV output power for Scenario 2 and 3, (c) Load profile for Scenario 2.

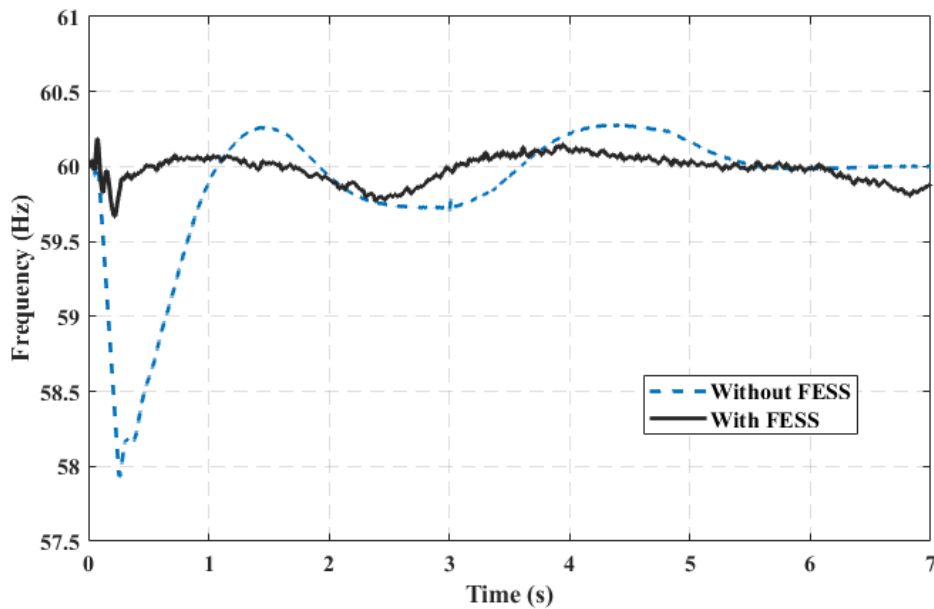


Figure 12. System frequency of Scenario 2.

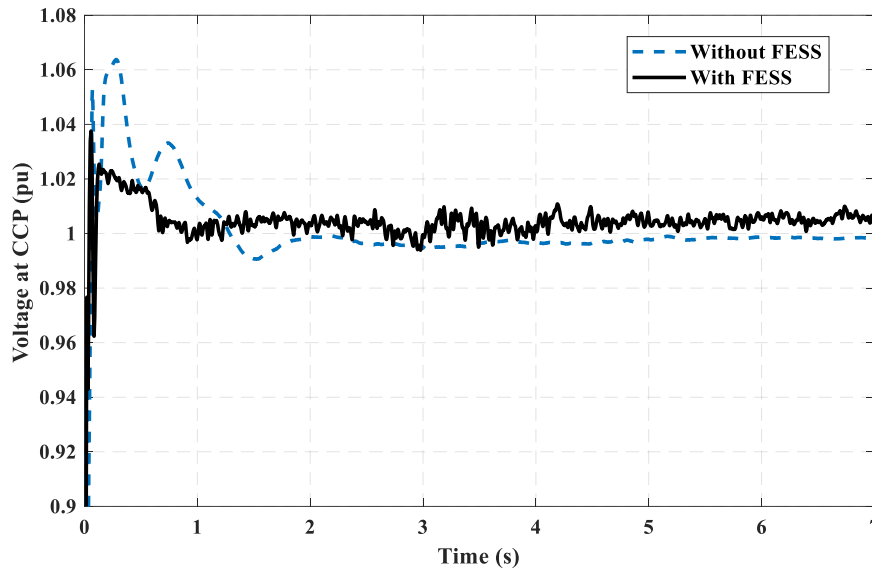


Figure 13. Voltage at CCP of Scenario 2.

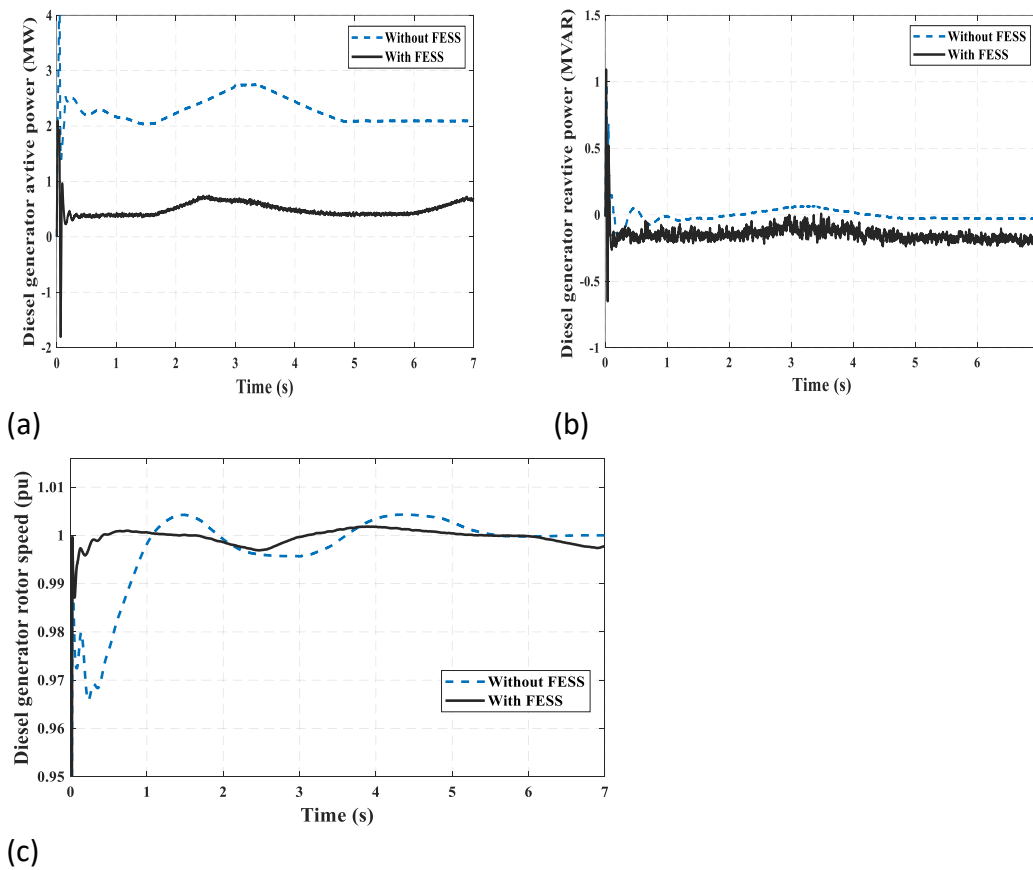


Figure 14. (a) Diesel generator active power of Scenario 2, (b) Diesel generator reactive power of Scenario 2, (c) Diesel generator rotor speed of Scenario 2.

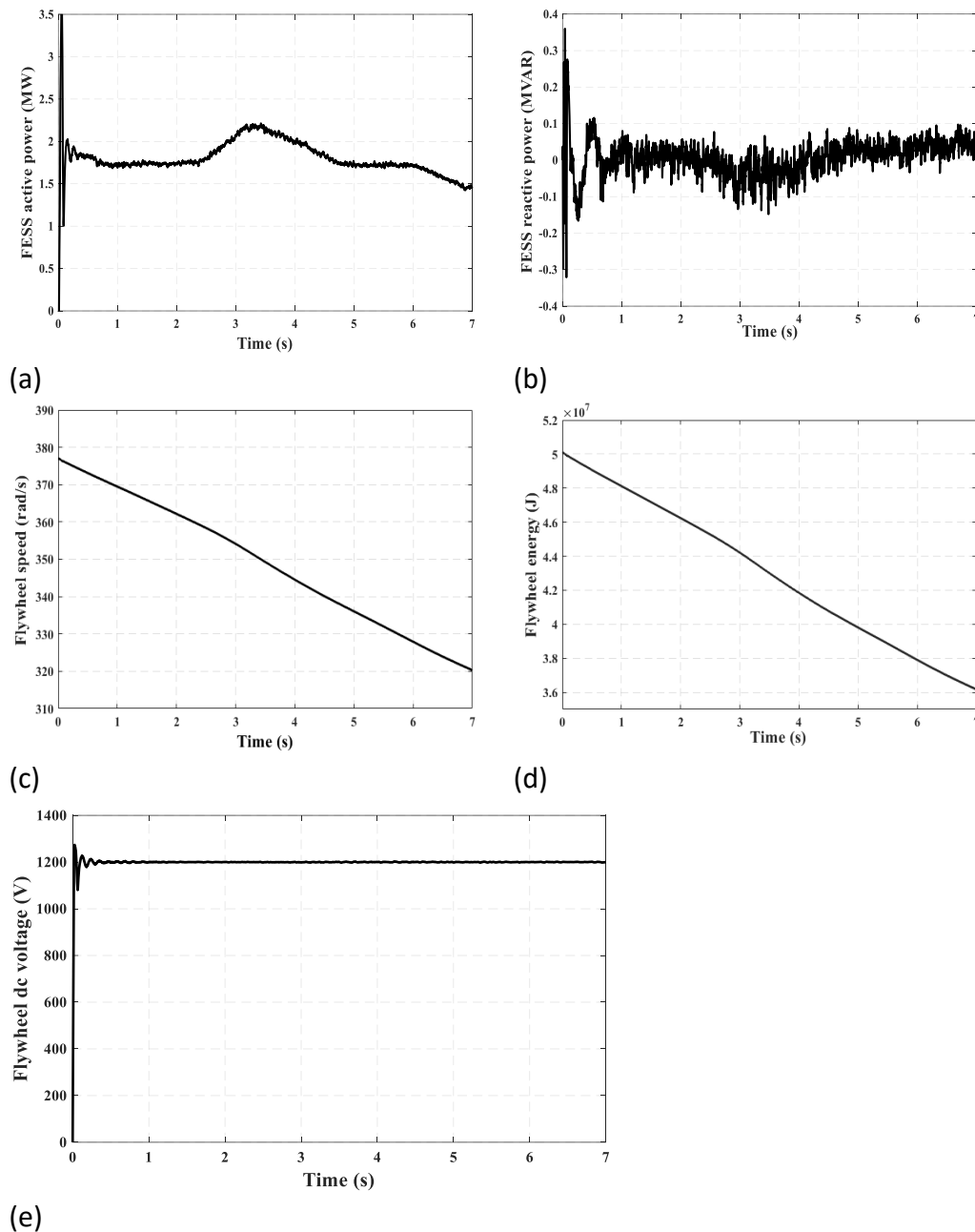


Figure 15. (a) FESS active power output of Scenario 2, (b) FESS reactive power output of Scenario 2, (c) Flywheel speed of Scenario 2, (d) FESS energy of Scenario 2, (e) Flywheel dc voltage of Scenario 2.

### Scenario 3

In this scenario, the load profile is shown in Figure 16, while the solar radiation and the PV output power are the same as in scenario 2. Figure 17 displays the system frequency. When the FESS is not being used, the frequency varies between 60.6 and 59.4 Hz during the abrupt load change. FESS successfully mitigated this variation to be around the rated value. Figure 18 displays the voltage at CCP. At a time of 4 s, the voltage fluctuates to 0.97 pu however, it is maintained at about 1.0 pu after employing FESS. Figures 19a - 19c display the diesel generator's active power, reactive power, and rotor speed, respectively. It is found that the diesel generator's active power share decreases to about 0.5 MW where the same amount of power is transferred via FESS. When reactive power is obtained by using FESS, the CCP voltage is controlled to 1.0 pu. When FESS is activated, the rotor speed is maintained at approximately 1.0 pu compared to a fluctuation between 1.012 pu and 0.99

pu without using FESS. Additionally, Figures 20a - 20e are used to show the active power, reactive power, energy, speed, and DC voltage of the FESS output. FESS contributes significantly to feeding and absorbing the excess power difference between generation and load. FESS responds rapidly when charging or discharging to account for any unforeseen variation in load demand.

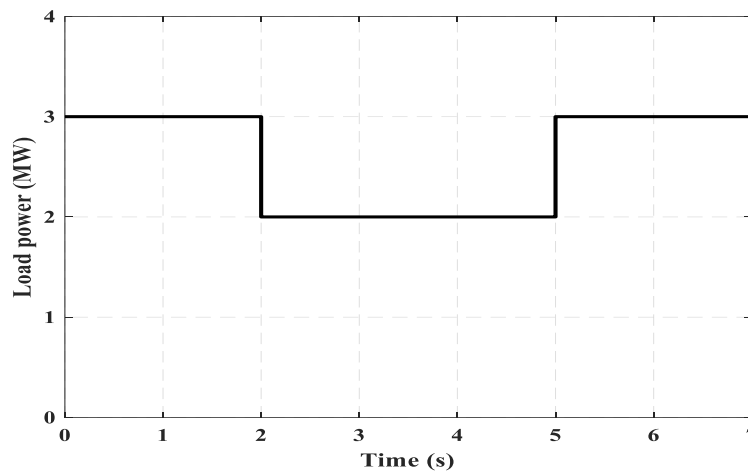


Figure 16. Load profile for Scenario 3.

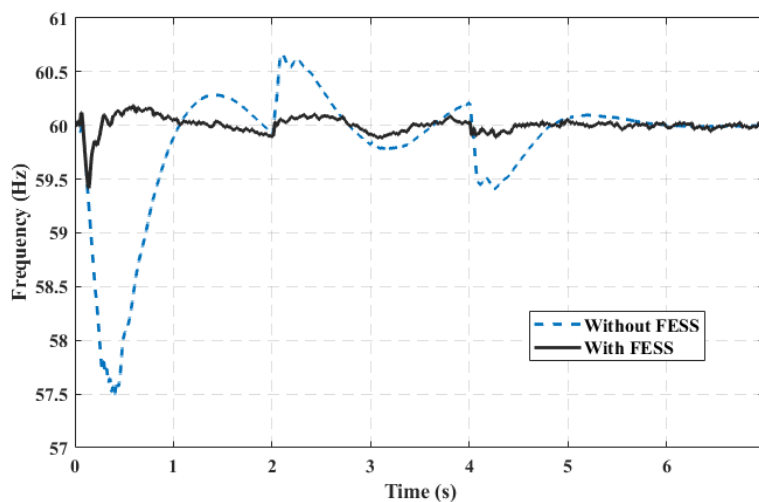


Figure 17. System frequency of Scenario 3.

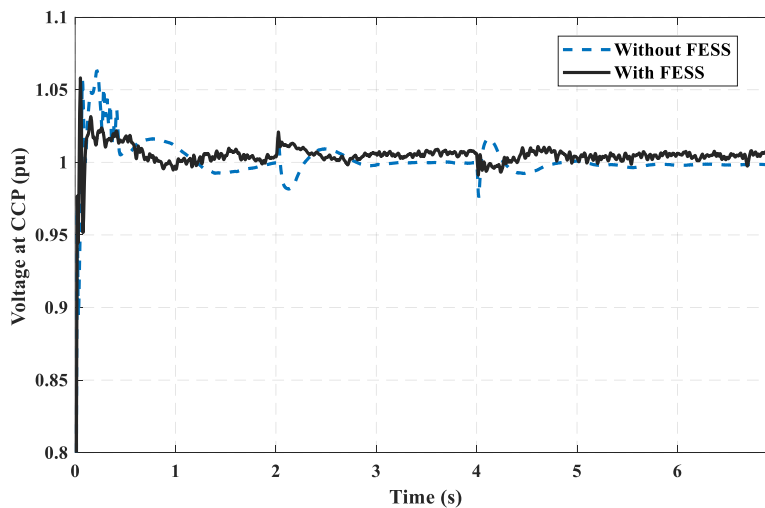


Figure 18. Voltage at CCP of Scenario 3.

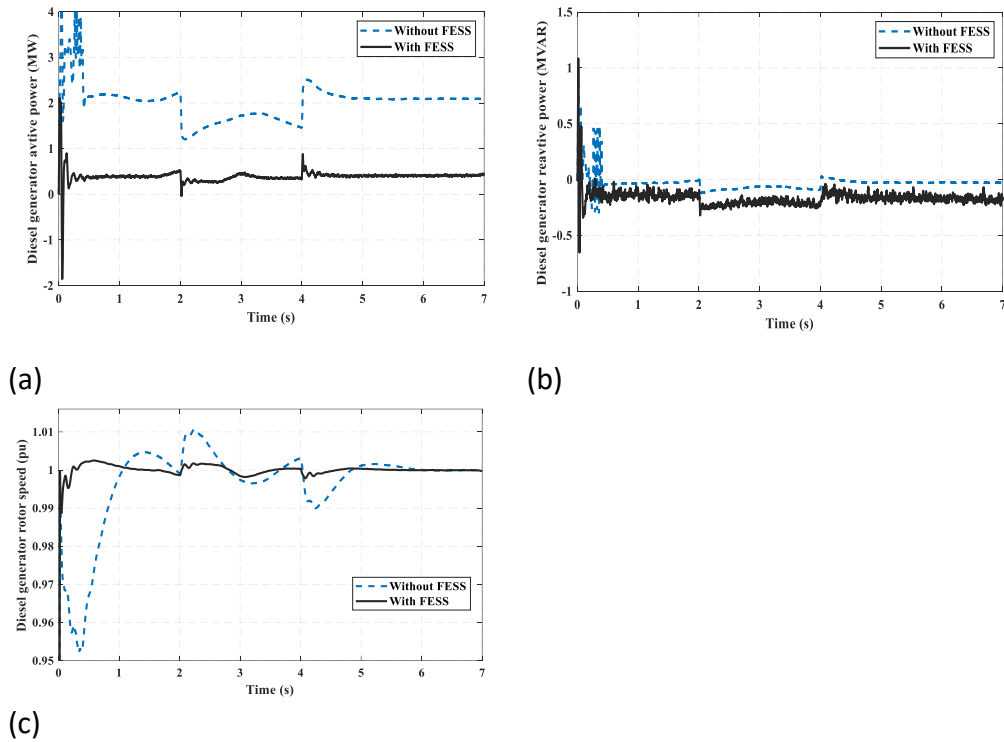


Figure 19. (a) Diesel generator active power of Scenario 3, (b) Diesel generator reactive power of Scenario 3, (c) Diesel generator rotor speed of Scenario 3.

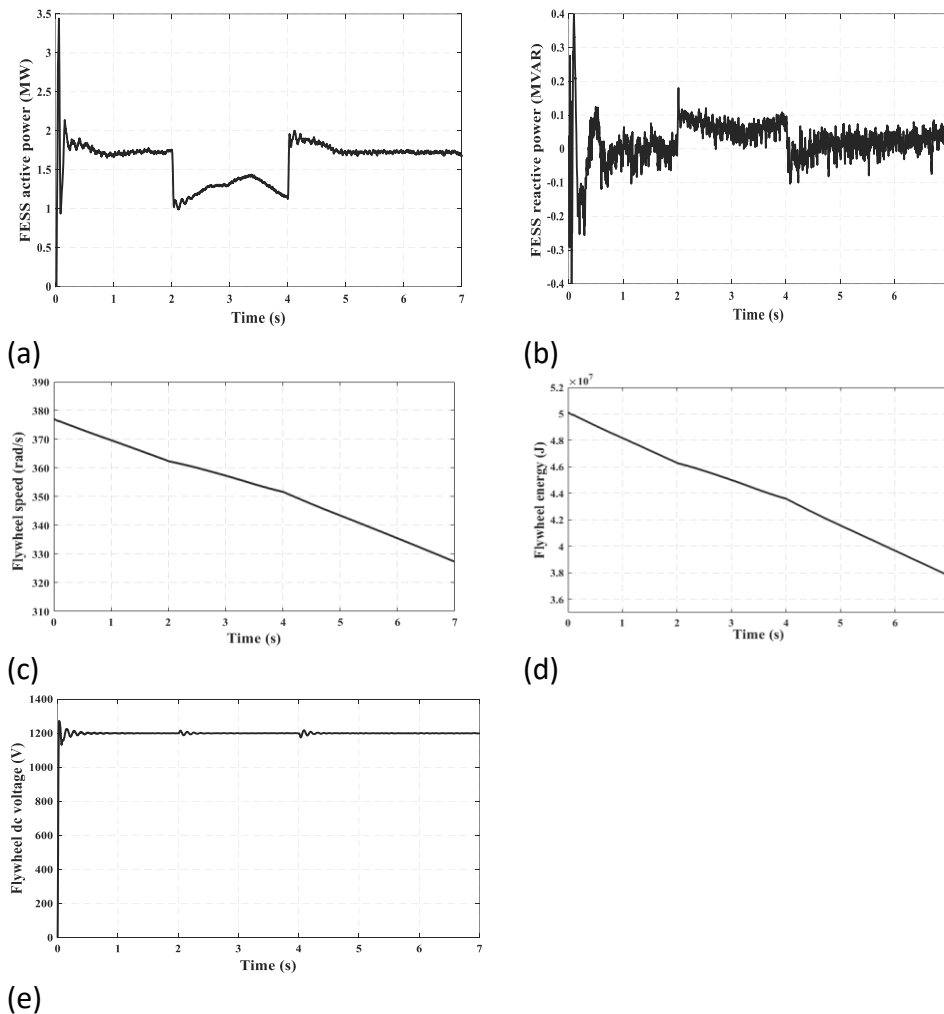


Figure 20. (a) FESS active power output of Scenario 3, (b) FESS reactive power output of Scenario 3. (c) Flywheel speed of Scenario 3. (d) FESS energy of Scenario 3, (e) Flywheel dc voltage of Scenario 3.

## Conclusion

This study proposes a developed control strategy for integrating FESS with RESs in an islanded MG, indicating their important role in addressing problems brought on by the intermittent nature of RESs. FESS has proven to help balance supply and demand load variations; it also enhanced the MG stability during the penetration of RESs. Power-sharing between PV, FESS, and diesel generators is managed by FLC to minimize system voltage and frequency oscillations caused by abrupt changes in load and/or PV output power. Three scenarios with and without FESS were tested to evaluate the proposed control strategy. The results indicated that voltage and frequency fluctuations have been minimized to be within the allowable limits, demonstrating that the FLC-based technique can regulate the power contributed by FESS. The minimum undershoot and maximum overshoot, mean value, and standard deviation for the MG system frequency and CCP voltage are provided in Table 4. The average value of the MG frequency for Scenario 1, Scenario 2, and Scenario 3 has improved by 5%, 10%, and 15%, respectively, by using FESS. On the other hand, with utilizing FESS, the CCP voltage is within acceptable standard limitations ( $\pm 5\%$  of the nominal value) for all three tested scenarios. The table shows that the proposed method can significantly reduce the minimum undershoot and the maximum overshoot of frequency and CCP voltage in the three proposed scenarios.

**TABLE 4. Improvement in frequency and voltage in the three scenarios.**

MG Frequency						
Scenario	Scenario 1		Scenario 2		Scenario 3	
	without FESS	with FESS	without FESS	with FESS	without FESS	with FESS
Minimum undershoot value	58.82	59.77	57.93	59.67	57.49	59.41
Maximum overshoot value	60.83	60.16	60.28	60.19	60.66	60.19
Mean value	59.95	60	59.88	59.98	59.85	60
Std (Standard deviation)	0.3703	0.06505	0.451	0.0901	0.5768	0.07584
Voltage at CCP						
Scenario	Scenario 1		Scenario 2		Scenario 3	
	without FESS	with FESS	without FESS	with FESS	without FESS	with FESS
Minimum undershoot value	0.977716	0.992584	0.991198	0.994438	0.976664	0.99214
Maximum overshoot value	1.06	1.052	1.064	1.038	1.063	1.050
Mean value	1.002	1.006	1.001	1.003	1.0	1.004
Std (Standard deviation)	0.03049	0.02951	0.03163	0.02894	0.03065	0.02906

## References

- Tran, Q.T.; Davies, K.; Sepasi, S. Isolation Microgrid Design for Remote Areas with the Integration of Renewable Energy: A Case Study of Con Dao Island in Vietnam. *Clean Technol.* 2021, 3, 828–844. <https://doi.org/10.3390/cleantechnol3040047>.
- Khan, N.; Kalair, E.; Abas, N.; Kalair, A.R.; Kalair, A. Energy Transition from Molecules to Atoms and Photons. *Eng. Sci. Technol. Int. J.* 2019, 22, 151–164. <https://doi.org/10.1016/j.jestch.2018.05.002>.
- Shahinzadeh, H.; Moazzami, M.; Fathi, S.H.; Gharehpetian, G.B. Optimal Sizing and Energy Management of a Grid-Connected Microgrid Using HOMER Software. In Proceedings of the 2016 Smart Grids Conference (SGC), Kerman, Iran, 20–21 December 2016; pp. 1–6. <https://doi.org/10.1109/SGC.2016.7882945>.

4. Hoarca, I.C.; Bizon, N.; Enescu, F.M. Using the Potential of Renewable Energy Sources in Romania to Reduce Environmental Pollution. In Proceedings of the *13th International Conference on Electronics, Computers and Artificial Intelligence (ECAI)*, Pitesti, Romania, 1–3 July 2021; pp. 1–6. <https://doi.org/10.1109/ECAI52376.2021.9515074>.
5. Jafarinejad, S.; Beckingham, B.S. Introduction to Renewable Energy–Water–Environment Nexus. In *The Renewable Energy-Water-Environment Nexus: Fundamentals, Technology, and Policy*; Elsevier: Amsterdam, The Netherlands, 2024; pp. 133–141.
6. Kotra, S.; Mishra, M.K. Design and Stability Analysis of DC Microgrid with Hybrid Energy Storage System. *IEEE Trans. Sustain. Energy* 2019, *10*, 1603–1612. <https://doi.org/10.1109/TSTE.2019.2891255>.
7. Esmailion. Hybrid Renewable Energy Systems for Desalination. *Appl. Water Sci.* 2020, *10*, 68. <https://doi.org/10.1007/s13201-020-1168-5>.
8. Said, S.M.; Salama, H.S.; Hartmann, B.; Vokony, I. A Robust SMES Controller Strategy for Mitigating Power and Voltage Fluctuations of Grid-Connected Hybrid PV–Wind Generation Systems. *Electr. Eng.* 2019, *101*, 1019–1032. <https://doi.org/10.1007/s00202-019-00848-z>.
9. Hemeida, A.M.; Hassan, M.R.; Hamdy, H. Maximizing Reliability of Two-Commodity Flow Networks with Time Constraint Using Fuzzy Optimization. *Aswan Univ. J. Sci. Technol.* 2022, *2*, 14–36.
10. Kumar, N.M.; Gorjian, S.; Shukla, A.B. Solar PV Module Technologies. In *Photovoltaic Solar Energy Conversion*; Academic Press: Cambridge, MA, USA, 2020; pp. 51–78.
11. Jäger-Waldau, A. Snapshot of Photovoltaics - February 2022. *EPJ Photovolt.* 2022, *13*, 1. <https://doi.org/10.1051/epjpv/2022010>.
12. Aleksandra, A.; Sara, B.P.; Małgorzata, J.; Brian, B.; Davide, P.; Miguel, C. Role of Solar PV in Net-Zero Growth: An Analysis of International Manufacturers and Policies. *Prog. Photovolt. Res. Appl.* 2024, *32*, 1–15. <https://doi.org/10.1002/pip.3797>.
13. Kaushik, E.; Prakash, V.; Mahela, O.P.; Khan, B.; El-Shahat, A.; Abdelaziz, A.Y. Comprehensive Overview of Power System Flexibility during the Scenario of High Penetration of Renewable Energy in Utility Grid. *Energies* 2022, *15*, 516. <https://doi.org/10.3390/en15020516>.
14. Sayed, E.T.; et al. Renewable Energy and Energy Storage Systems. *Energies* 2023, *16*, 1415. <https://doi.org/10.3390/en16031415>.
15. Bahnasawy, A.E.; Ali, S. Improving the Dynamic Performance of Two-Area System Based Integration of RES. *Aswan Univ. J. Sci. Technol.* 2024, *4*, 106–119. <https://doi.org/10.21608/aujst.2024.270294.1083>.
16. Olabi, A.G.; Wilberforce, T.; Abdelkareem, M.A.; Ramadan, M. Critical Review of Flywheel Energy Storage System. *Energies* 2021, *14*, 2159. <https://doi.org/10.3390/en14082159>.
17. Choudhury, S. Flywheel Energy Storage Systems: A Critical Review on Technologies, Applications, and Future Prospects. *Int. Trans. Electr. Energy Syst.* 2021, *31*, e13024. <https://doi.org/10.1002/2050-7038.13024>.
18. Yu, Q.; Tian, L.; Li, X.; Tan, X. Compressed Air Energy Storage Capacity Configuration and Economic Evaluation Considering the Uncertainty of Wind Energy. *Energies* 2022, *15*, 4637. <https://doi.org/10.3390/en15134637>.
19. Falcone, M.; Rehman, D.; Dongellini, M.; Naldi, C.; Pulvirenti, B.; Morini, G.L. Experimental Investigation on Latent Thermal Energy Storages (LTESs) Based on Pure and Copper-Foam-Loaded PCMs. *Energies* 2022, *15*, 4894. <https://doi.org/10.3390/en15134894>.
20. Tadesse, M.G.; Kasaw, E.; Fentahun, B.; Loghin, E.; Lübben, J.F. Banana Peel and Conductive Polymers-Based Flexible Supercapacitors for Energy Harvesting and Storage. *Energies* 2022, *15*, 2471. <https://doi.org/10.3390/en15072471>.

21. Alnaqbi, S.A.; Alasad, S.; Aljaghoub, H.; Alami, A.H.; Abdelkareem, M.A.; Olabi, A.G. Applicability of Hydropower Generation and Pumped Hydro Energy Storage in the Middle East and North Africa. *Energies* 2022, *15*, 2412. <https://doi.org/10.3390/en15072412>.
22. Xu, K.; Guo, Y.; Lei, G.; Zhu, J. A Review of Flywheel Energy Storage System Technologies. *Energies* 2023, *16*, 6462. <https://doi.org/10.3390/en16186462>.
23. Arani, A.A.K.; Karami, H.; Gharehpetian, G.B.; Hejazi, M.S.A. Review of Flywheel Energy Storage Systems Structures and Applications in Power Systems and Microgrids. *Renew. Sustain. Energy Rev.* 2017, *69*, 9–18. <https://doi.org/10.1016/j.rser.2016.08.031>.
24. Faisal, M.; Hannan, M.A.; Ker, P.J.; Hussain, A.; Mansor, M.B.; Blaabjerg, F. Review of Energy Storage System Technologies in Microgrid Applications: Issues and Challenges. *IEEE Access* 2018, *6*, 35143–35164. <https://doi.org/10.1109/ACCESS.2018.2841407>.
25. El-Deeb, H.M.; Daoud, M.I.; Elserougi, A.; Abdel-Khalik, A.S.; Ahmed, S.; Massoud, A.M. Maximum Power Transfer of PV-Fed Inverter-Based Distributed Generation with Improved Voltage Regulation Using Flywheel Energy Storage Systems. In *Proceedings of the IECON 2014 - 40th Annual Conference of the IEEE Industrial Electronics Society*, Dallas, TX, USA, 2014; pp. 3135–3141. <https://doi.org/10.1109/IECON.2014.7048958>.
26. Ji, W.; et al. Applications of Flywheel Energy Storage System on Load Frequency Regulation Combined with Various Power Generations: A Review. *Renew. Energy* 2024, *223*, 119975. <https://doi.org/10.1016/j.renene.2024.119975>.
27. Abbezzot, C.; Tran, T.; Poggi, P.; Serre-Combe, P.; Perrin, M.; Muselli, M. Using a Flywheel Associated to PV Power Plant in Order to Increase the Integration of PV into Island Electrical Grid. *Renew. Energy Power Qual. J.* 2013, *1*, 11. <https://doi.org/10.24084/repqj11.370>.
28. Wang, Y.; Zhang, J.; Liu, G. Model Predictive Control of Matrix Converter-Based Flywheel Energy Storage System. In *Proceedings of the 2021 IEEE International Conference on Predictive Control of Electrical Drives and Power Electronics (PRECEDE)*, Jinan, China, 2021; pp. 819–824. <https://doi.org/10.1109/PRECEDE51386.2021.9680913>.
29. Macit, E.; Vural, A.M. Modelling and Simulation of 1 MW Grid-Connected PV System Regulated by Sliding Mode Control, Model Predictive Control and PI Control. *Gazi Univ. J. Sci.* 2022, *35*, 899799. <https://doi.org/10.35378/gujs.899799>.
30. Hassan, M.A.; et al. Evaluation of Energy Extraction of PV Systems Affected by Environmental Factors under Real Outdoor Conditions. *Theor. Appl. Climatol.* 2022, *150*, 1–2. <https://doi.org/10.1007/s00704-022-04166-6>.
31. Ghoniem, R.M.; Alahmer, A.; Rezk, H.; As'ad, S. Optimal Design and Sizing of Hybrid Photovoltaic/Fuel Cell Electrical Power System. *Sustainability* 2023, *15*, 12026. <https://doi.org/10.3390/su151512026>.
32. Al-Chaderchi, M.; Sopain, K.; Alghoul, M.A.; Salameh, T. Experimental Study of the Effect of Fully Shading on the Solar PV Module Performance. In *E3S Web Conf.* 2017, *23*, 01001. <https://doi.org/10.1051/e3sconf/20172301001>.
33. Dubey, K.; Shah, M.T. Design and Simulation of Solar PV System. In *Proceedings of the 2016 International Conference on Automatic Control and Dynamic Optimization Techniques (ICACDOT)*, Pune, India, 2016; pp. 568–573. <https://doi.org/10.1109/ICACDOT.2016.7877649>.
34. Kathe, M.L.; Makokha, A.B.; Zachary, S.O.; Adaramola, M.S. A Comprehensive Review of Maximum Power Point Tracking (MPPT) Techniques Used in Solar PV Systems. *Energies* 2023, *16*, 2206. <https://doi.org/10.3390/en16052206>.
35. Zobair, M.; Aly, M.M.; Said, S.M. Mitigation of Voltage and Frequency Oscillations of a Microgrid during Wind Gust by Using Fuzzy-Controlled Flywheel Energy Storage. *Int. J. Appl. Energy Syst.* 2024, *6*, 12–22. <https://doi.org/10.21608/IJAES.2023.221324.1020>.

36. Olabi, A.G.; Wilberforce, T.; Abdelkareem, M.A.; Ramadan, M. Critical Review of Flywheel Energy Storage System. *Energies* 2021, *14*, 82159. <https://doi.org/10.3390/en14082159>.
37. Amiryar, M.E.; Pullen, K.R. Assessment of the Carbon and Cost Savings of a Combined Diesel Generator, Solar Photovoltaic, and Flywheel Energy Storage Islanded Grid System. *Energies* 2019, *12*, 173356. <https://doi.org/10.3390/en12173356>.
38. Bihari, S.P.; et al. A Comprehensive Review of Microgrid Control Mechanism and Impact Assessment for Hybrid Renewable Energy Integration. *IEEE Access* 2021, *9*, 88942–88958. <https://doi.org/10.1109/ACCESS.2021.3090266>.
39. Cendoya, M.G.; Toccaceli, G.M.; Battaiotto, P.E.; Vignoni, R.J. Microgrid for Remote Areas with Water Pumping, Based on Wind-Diesel DER and Energy Storage. In *Proceedings of the 2015 IEEE PES Innovative Smart Grid Technologies Latin America (ISGT LATAM)*, Montevideo, Uruguay, 2015; pp. 154–159. <https://doi.org/10.1109/ISGT-LA.2015.7381145>.
40. Jin, C.; Jiang, X.; Zhong, G.; Li, X. Research on Coordinated Control Strategy of Flywheel Energy Storage Array for Island Microgrid. In *Proceedings of the 2017 IEEE Conference on Energy Internet and Energy System Integration (EI2)*, Beijing, China, 2017; pp. 1–6. <https://doi.org/10.1109/EI2.2017.8245616>.
41. Calero, F.; et al. A Review of Modeling and Applications of Energy Storage Systems in Power Grids. *Proc. IEEE* 2023, *111*, 806–831. <https://doi.org/10.1109/JPROC.2022.3158607>.
42. Buchroithner, A.; et al. Decentralized Low-Cost Flywheel Energy Storage for Photovoltaic Systems. In *Proceedings of the 2016 International Conference on Sustainable Energy Engineering and Application (ICSEEA)*, Jakarta, Indonesia, 2016; pp. 41–49. <https://doi.org/10.1109/ICSEEA.2016.7873565>.
43. Said, S.; Aly, M.; Hartmann, B. A Robust SMES Control for Enhancing Stability of Distribution Systems Fed from Intermittent Wind Power Generation. *Turk. J. Electr. Eng. Comput. Sci.* 2019, *27*, 1810. <https://doi.org/10.3906/elk-1810-10>.
44. Attia, H. Fuzzy Logic Controller Effectiveness Evaluation through Comparative Memberships for Photovoltaic Maximum Power Point Tracking Function. *Int. J. Power Electron. Drive Syst.* 2018, *9*, 3. <https://doi.org/10.11591/ijpeds.v9>.
45. Yasin, A.M.; Alsayed, M.F. Fuzzy Logic Power Management for a PV/Wind Microgrid with Backup and Storage Systems. *Int. J. Electr. Comput. Eng.* 2021, *11*, 2876–2888. <https://doi.org/10.11591/ijece.v11i4.pp2876-2888>.
46. Salama, H.S.; Said, S.M.; Vokony, I.; Hartmann, B. Adaptive Coordination Strategy Based on Fuzzy Control for Electric Vehicles and Superconducting Magnetic Energy Storage—Towards Reliably Operating Utility Grids. *IEEE Access* 2021, *9*, 61662–61670. <https://doi.org/10.1109/ACCESS.2021.3074578>.
47. Ben Smida, M.; Sakly, A. Fuzzy Logic Control of a Hybrid Renewable Energy System: A Comparative Study. *Wind Eng.* 2021, *45*, 4. <https://doi.org/10.1177/0309524X211028783>.
48. Said, S.M.; Hartmann, B. A Robust Controlled-SMES for Islanding Microgrid Distribution Systems. In *Proceedings of the 2018 6th International Istanbul Smart Grids and Cities Congress and Fair (ICSG)*, 2018; pp. 139–143. <https://doi.org/10.1109/SGCF.2018.8408959>.